Analysis of a Nonisothermal Simulated Moving-Bed Reactor

Jin Xu and Yuming Liu
College of Chemistry and Materials Engineering, Wenzhou University, Chashan University Town, Wenzhou 325035, Zhejiang, China

Guoqian Xu
Bayer Technology and Engineering (Shanghai) Co., Ltd., Shanghai Chemical Industry Park, Shanghai 201507, China

Weifang Yu
College of Chemistry and Materials Engineering, Wenzhou University, Chashan University Town, Wenzhou 325035, Zhejiang, China

Ajay K. Ray
Dept. of Chemical and Biochemical Engineering, University of Western Ontario, London, ON, N6A 5B9, Canada

DOI 10.1002/aic.14216
Published online September 12, 2013 in Wiley Online Library (wileyonlinelibrary.com)

Simulated moving-bed reactor (SMBR) is a multifunctional reactor wherein in situ *separation of the products facilitates the reversible reaction to completion beyond thermodynamic equilibrium and at the same time obtaining products of high purity. In this work, we investigate the feasibility of introducing variances in adsorption strength, which has recently been proven to effectively improve SMB performance for pure separation, into an SMB system to include reactions. Synthesis of methyl acetate catalyzed by amberlyst 15 is considered as model system. Numerical simulations were carried out for an SMBR unit consisting of four columns and operated with various temperature distributions in the range of 308–323 K. SMBR productivities were evaluated and compared under the constraints of complete conversion and complete product separation. The effects of kinetics, heat transfer efficiency and adsorption strength of reactant were systematically investigated.* © 2013 American Institute of Chemical Engineers *AIChE J*, 59: 4705–4714, 2013
Keywords: reactor analysis, simulation, process, chromatography (LC and SMB), absortion, modeling

Introduction

The technique of simulated moving-bed reactor (SMBR) integrates chemical reaction and adsorptive separation in a single apparatus. The onsite separation of products enhances the conversion of thermodynamically limited reactions and simplifies the downstream after-treatment for product purification. In addition, SMBR is continuously operated and is easy to implement in practice, compared with a true moving bed (TMB) system, because the latter involves movement of solid adsorbent which brings in a number of problems, such as mechanical difficulties of moving the solid, adsorbent attrition, fines removal, flow channeling, etc. Studies have been carried out to investigate SMBR applications on various reactions such as esterification,[1–4] etherification,[5] hydrogenation,[6,7] and isomerization,[8,9] as well as those involving sugar.[10,11] It has received growing interests in recent years for the production and preparation of some fine chemicals and pharmaceuticals,[12] where reactive distillation process might not be suitable, since some of the chemical species involved are nonvolatile and/or temperature sensitive.

Correspondence concerning this article should be addressed to A. K. Ray at aray@eng.uwo.ca.

Figure 1 shows the schematic diagram of a typical SMBR in which a reversible reaction $A \leftrightarrow B + C$, is carried out. The continuous operation of SMBR is realized by periodically switching the ports connecting a number of reactive chromatography columns. Given appropriate switching time and flow rates, the mobile phase has an overall movement toward the clockwise direction with respect to the ports. The inlet and outlet ports divide the SMBR unit into 4 zones, each playing a specific functional role. Reactant (A) is conveyed by the solvent (S) and fed into the system, where the reaction is activated forming B and C. The products, B and C, are selectively adsorbed on the stationary phase. The preferentially (strongly) adsorbed species B moves with the solid phase toward zone II and is collected at the extract port, while the less (weekly) adsorbed species C moves with the mobile phase toward zone III and is collected at the raffinate port. Reaction and separation mainly occur in zones II and III. Zones I and IV are for the regeneration of solid and mobile phases, respectively. Under properly controlled operating conditions, complete conversion and pure products of both B and C can be simultaneously achieved.

Due to the existence of chemical reactions, SMBR is more complicated than SMB, a pure separation process. Lode et al.[13] theoretically investigated the effects of design parameters on the performance of an SMBR operated in the linear

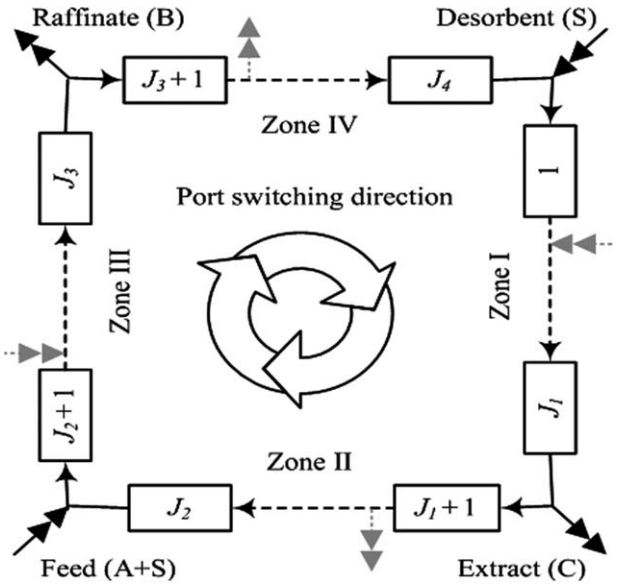

Figure 1. Schematic diagram of an SMBR.

Black and gray arrows are port positions at current and the next switches, respectively.

range. It was also pointed out that TMB model does not apply to the numerical analysis of SMBR units with a practically reasonable number of columns, which is not the case for SMB processes. This study was then extended to nonlinear conditions with more attentions focused on the influence of feed composition.[14] In our previous studies, we found that some of the key operating parameters, such as switching time, column distribution and flow rates in different zones, have contradicting effects on SMBR productivity and product purity.[10] The design of SMBR processes, therefore, involves a multiobjective optimization problem, which can be systematically solved using genetic algorithm (GA).[15,16]

Efficiency of the onsite separation has substantial effects on the performance of an SMBR. Several recently developed techniques, e.g., VariCol, PowerFeed and ModiCon, for the improvement of pure SMB separation also have potential applications in reactive processes.[16–18] It has been shown in our previous studies that SMBRs incorporated with VariCol and PowerFeed perform better than traditional SMB operation mode due to increased flexibility in the adaptable operating parameters.[16,19]

Conventional SMB and SMBR processes are operated under isothermal and isocratic conditions. More recently, studies have been carried out to improve SMB performance by adjusting adsorption behaviors in each operating zone according to its function. It has been shown that a gradient of adsorption strength ascending from zone I to zone IV, which can be realized by establishing a gradient of temperature[20,21] or eluent composition,[22,23] can significantly enhance the productivity of SMB processes.

The objective of this work is to investigate the feasibility of introducing variances in adsorption strength into an SMBR unit. To our knowledge, this is the first attempt in this area. We investigated theoretically the thermal effects on SMBR productivity. For this purpose, the synthesis of methyl acetate catalyzed by amberlyst 15 was used as the model reaction. The article is organized as follows. After this introduction section, the catalytic reaction of methyl acetate synthesis is first briefly introduced. Then a mathematic model accounting for separation, reaction, and thermal effects is developed, followed by a description of the calculation procedure. Calculation results are presented and discussed in detail. Calculated temporal and spatial component profiles are used to elucidate some of the important qualitative trends. Finally, conclusions are given.

Model description

Synthesis of Methyl Acetate. Methyl acetate (E) is produced by the liquid-phase reaction of acetic acid (A) and methanol (M) with water (W) being the byproduct. The overall reaction is

$$A+M \leftrightarrow E+W \tag{1}$$

The reaction is reversible and the conversion is equilibrium-limited. This work was focused on the forward esterification reaction, and, hence, methanol was used as the carrier solvent present in much excess. In this case, it may be assumed that concentration of methanol and volumetric flow rate in a column are constant and independent of the reaction progress. Since the concentration of methanol is constant, in the point view of process analysis, reaction (1) falls into the catalogue of reactions in the form of $A \leftrightarrow B+C$ that has been described earlier in the Introduction.

The synthesis of methyl acetate in isothermal and isocratic SMBRs packed with amberlyst 15 solid phase has been systematically investigated (both theoretically and experimentally) in our previous studies.[10,15,24] It was shown that complete conversion of A and complete separation of E and W can be simultaneously achieved under proper operating conditions. SMBR productivity can be significantly improved by the use of VariCol technique. The investigation is extended to nonisothermal operations in this work.

SMBR Model. Equilibrium-dispersive (ED) model[25,26] has been widely used to describe the component mass balance in theoretical studies of simulated moving-bed chromatography processes. It was extended in this work to include catalytic reaction and thermal effects

$$\frac{\partial c_{i,j}}{\partial t}+\varphi\frac{\partial q_{i,j}}{\partial t}+u_{\text{int},j}\frac{\partial c_{i,j}}{\partial z}-\varphi_j\upsilon_i r=D_{app,i,j}\frac{\partial^2 c_{i,j}}{\partial z^2} \tag{2}$$

$$q_i \equiv q_i^*=f_i(c,T) \tag{3}$$

$$r=g(q,T) \tag{4}$$

where c and q are concentrations in the mobile and stationary phases, i and j are indices of component and column, t is time, φ is phase ratio related to column vacancy by $\varphi=\frac{1-\varepsilon}{\varepsilon}$, u_{int} is the interstitial velocity of mobile phase, z is axial coordinate, D_{app} is apparent axial dispersion coefficient accounting for molecular diffusion, eddy diffusion and mass transfer effects, υ is stoichiometric number in the reaction (positive for reactant), T is temperature, f and g are local functions defining the adsorption equilibrium and catalytic reaction rate, respectively.

In order to efficiently solve the above model, we used the Martin-Synge method[27,28] that replaces the second derivative ($\frac{\partial^2}{\partial z^2}$ term) in Eq. 2 with truncation error brought in by the first-order backward approximation of $\frac{\partial}{\partial z}$ (numerical dispersion)

$$\frac{c_i(z)-c_i(z-\Delta z)}{\Delta z}=\left.\frac{\partial c_i}{\partial z}\right|_z-\left.\frac{\partial^2 c_i}{\partial z^2}\right|_z\frac{\Delta z}{2}+O\left(\Delta z^2\right) \tag{5}$$

$$\Delta z=\frac{2D_{app}}{u_{\text{int}}}=\frac{L}{N} \tag{6}$$

where N is the plate number. For simplicity, it was assumed in this study that the value of N is same for all components in all

Table 1. Model Parameters used in the Calculations

Column [a]			Adsorption equilibrium [b]		Kinetics [b]	
L /m	0.025		H^0	ΔH_{ads}/ kJ·mol^{-1}	k_f^0/s^{-1}	3.26×10^5
d /m	9.4×10^{-3}	A	2.53×10^{-4}	−19.64	E_f/kJ·mol^{-1}	44.2
ε	0.4	E	0.012	−9.10	K_{eq}^0/ mol m^{-3}	3.69×10^7
N	50	W	0.116	−8.53	ΔH_{rxn}/kJ·mol^{-1}	−5.83

[a]column parameters in consistence with ref. 10 and 15;
[b]adsorption and kinetic parameters determined in ref. 24.All parameters are in consistent with the previous publication

columns.[29] The aforementioned numerical scheme was shown to be accurate and efficient for the solution of both ED[27] and TD (transport-dispersive)[28] chromatography models. Substituting Eqs. 5 and 6 into Eq. 2 and neglecting $O(\Delta z^2)$ gives

$$\frac{\partial c_{i,j,M}}{\partial t}+\varphi\frac{\partial q_{i,j,M}}{\partial t}+u_{\text{int},j}\frac{c_{i,j,M}-c_{i,j,M-1}}{\Delta z}-\varphi_j\upsilon_i r=0 \quad (7)$$

where M denotes the mesh points ($M=0$ for the inlet and $M=N$ for the outlet). Since the second-order derivative is eliminated from Eq. 7, only inlet boundary condition is retained and is given by the node balance[10,15,24]

$$\text{Desorbent node}: Q_D=Q_I-Q_{IV};\ c_{i,in,I}=\frac{c_{i,D}Q_D+c_{i,out,IV}Q_{IV}}{Q_I} \quad (8)$$

$$\text{Extract node}: Q_{Ex}=Q_I-Q_{II};\ c_{i,in,II}=c_{i,out,I} \quad (9)$$

$$\text{Feed node}: Q_F=Q_{III}-Q_{II};\ c_{i,in,III}=\frac{c_{i,F}Q_F+c_{i,II}Q_{II}}{Q_{III}} \quad (10)$$

$$\text{Raffinate node}: Q_{Ra}=Q_{III}-Q_{IV};\ c_{i,in,IV}=c_{i,out,III} \quad (11)$$

where Q is the volumetric flow rate, subscripts D, Ex, F and Ra donate desorbent, extract, feed and raffinate, respectively (see Figure 1).

In general, energy balance equations should be included in the model and solved together with the mass balance equations. Following the suggestion by Migliorini et al.[20] spatial temperature gradient within a chromatographic column was neglected in this theoretical study for simplicity. In addition, the column temperature was assumed to change exponentially after a switch

$$T_j=T_j^\infty+\left(T_{jpre}^\infty-T_j^\infty\right)\exp(-\lambda t) \quad (12)$$

T_j^∞ is the final temperature of the current switch preset for column j, is a positive constant characterizing the transient temperature change, t is reset to 0 after each switch operation, $jpre = I$ for $j = IV$ and $jpre = j + 1$ for other columns. In this study, a value of 1.67×10^{-2} s^{-1} was assigned to λ unless otherwise mentioned. It should be noted that the exponential profile was used in this study mainly because it is smooth, bounded in the correct range, and, more importantly, it is a monotonic function of time with a continuously decelerating rate, which is likely the case during the transition period. In addition, it's simple form with a single parameter of λ is preferred during the investigation of transition period effects that will be discussed later in this article. In the literatures, exponential evolution of a variable is not uncommon in the modeling of a process operated under periodically changed conditions.[30,31] While it is acknowledged that temporal and spatial temperature profile during the transition period of realistic operations may be more complex than the description of Eq. 12, we believe that the use of Eq. 12 does give qualitatively correct trends that are pursued in this study.

Model Parameters. Amberlyst 15 has two major functions crucial for the successful operation of an SMBR (1) it catalyzes the esterification reaction, and (2) preferentially adsorbs water over acid and ester. Both kinetics and adsorption equilibrium have been investigated in our previous study.[24] Some of results are summarized in the following.

Henry's law applies for the adsorption of A, E and W, on the stationary phase

$$q_i^*=H_i c_i \cdot i=A,E,W \quad (13)$$

where H is Henry's constant. The rate of catalytic reaction (1) can be described as

$$r=k_f\left(q_A-\frac{q_E q_W}{K_{eq}}\right) \quad (14)$$

where k_f is the forward rate constant, and K_{eq} is the equilibrium constant. Since methanol is used as the solvent and in much excess, its component mass balance equation is not included in the model and the kinetic effects are included in the rate and equilibrium constants.

In the case of independent linear adsorption, Eq. 7 can be rewritten as

$$\left(1+\varphi_j H_i\right)\frac{\partial c_{i,j,M}}{\partial t}+\varphi_j c_{i,j}\frac{\partial H_i}{\partial T}\left(\frac{\partial T}{\partial t}\right)_j+u_{\text{int},j}\frac{c_{i,j,M}-c_{i,j,M-1}}{\Delta z}-\varphi_j\upsilon_i r=0 \quad (15)$$

H, k_f and K_{eq} are functions of temperature

$$H_i=H_i^0\exp\left(-\frac{\Delta H_{ads,i}}{RT}\right) \quad (16)$$

$$k_f=k_f^0\exp\left(-\frac{E_f}{RT}\right) \quad (17)$$

$$K_{eq}=K_{eq}^0\exp\left(-\frac{\Delta H_{rxn}}{RT}\right) \quad (18)$$

where R is the universal gas constant, H_i^0, k_f^0 and K_{eq}^0 are pre-exponential constants, E_f is activation energy of the forward reaction, ΔH_{ads} and ΔH_{rxn} are enthalpies of adsorption and reaction, respectively. Model parameters used in the calculations are summarized in Table 1.

Procedure. In order to proceed, some important variables are first introduced below.

Product water (W) is preferentially adsorbed and collected in the extract (Ex) port, whereas methyl acetate (E) is less adsorbed and collected in raffinate (Ra) port. In this work, an arbitrarily high value of 99.5% was imposed on the average purity of both products at cyclic steady-states

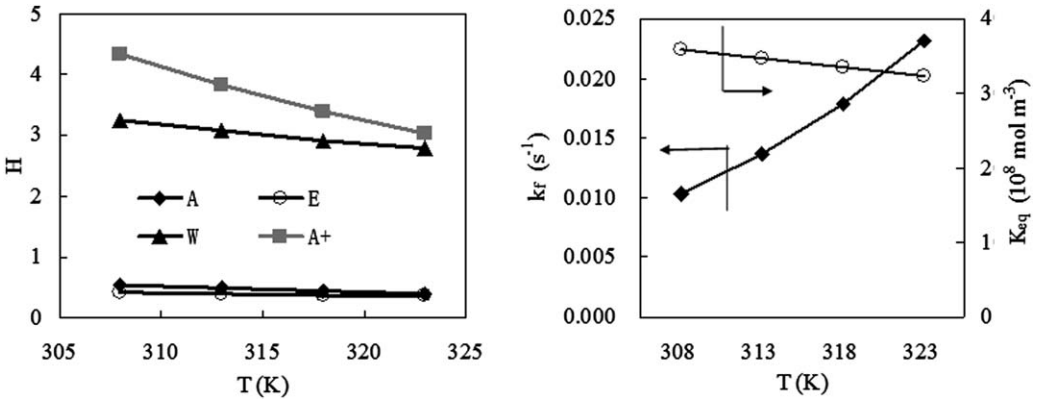

Figure 2. Temperature effects on H, k_f and K_{eq}. A+ means that Henry's constant of A is multiplied by 8 (used in the discussion of adsorption strength effects).

$$Pur_E = \frac{\int_0^{t_s} c_{E,Ra}\ dt}{\int_0^{t_s} \left(c_{A,Ra}+c_{E,Ra}+c_{W,Ra}\right) dt} \geq 99.5\% \quad (19)$$

$$Pur_W = \frac{\int_0^{t_s} c_{W,Ex}\ dt}{\int_0^{t_s} \left(c_{A,Ex}+c_{E,Ex}+c_{W,Ex}\right) dt} \geq 99.5\% \quad (20)$$

Since Eqs. 19 and 20 include acid concentration term in denominators, they not only provide standards for complete product separation, but also present constraints for practically complete acid conversion. Given constraints for complete conversion and separation, fixed column configuration, and fixed feed/desorbent composition, the productivity can be conveniently evaluated using Q_F.

Flow rate ratios in different operating zones are widely used in the SMB analyses. They are defined as

$$m_j = \frac{Q_j t_s - V_{col}\varepsilon}{V_{col}(1-\varepsilon)} \quad (21)$$

Each SMB zone, in order to fulfill its functional role described earlier, must be properly operated to satisfy certain criteria, which can be given in terms of the corresponding m value.[30] Zones I and IV are for the regeneration of adsorbent and solvent, respectively. Under ideal conditions, namely, infinite plate number, instantaneous and linear adsorption equilibrium, the criteria for complete separation are[32]

$$m_I \geq H_A \quad (22)$$

$$m_{IV} \leq H_B \quad (23)$$

where A and B denote the stronger and weaker adsorbates, respectively. In our study, a realistic SMBR model was used to describe the column with a finite number of theoretical plates. The nonideality was accounted for by the use of constant conservative multipliers in m_I and m_{IV}

$$m_I = H_w(T_I) \times 1.3 \quad (24)$$

$$m_{IV} = H_E(T_{IV})/2.0 \quad (25)$$

The choice of these multiplier values will be justified later in the discussion section.

Due to the incorporation of chemical reactions, an SMBR is more complicated than SMB for pure separation, even in the linear adsorption range. In this study, SMBR simulations were carried out to identify suitable operating region in the (m_{II} - m_{III}) plane for various temperature distributions in the 4 zones. The calculation procedure for each temperature distribution is described as follows:

1. Q_I is the largest among the mobile phase flow rates in the four zones and is generally set at a high value allowed by the maximum pressure drop of a chromatography column.[10,15,16,26] It was fixed at 5×10^{-8} m^3/s, consistent with our previous experimental and theoretical studies[10,15]; t_s was then calculated using the assigned operating temperature of zone I and Eqs. 21 and 24;
2. Q_{IV} was calculated using the assigned operating temperature of zone IV and Eqs. 21 and 25;
3. Using the column and kinetic models described in the previous sections, SMBR simulations were carried out along straight lines parallel to the diagonal in the (m_{II} - m_{III}) plane; m_{II} and m_{III} were converted to Q_{II} and Q_{III} using Eq. 21;
4. The complete conversion and separation zone in the (m_{II} - m_{III}) plane was identified to meet the constraints given in Eqs. 19 and 20.

The vertices (optimal operating points) of the complete conversion and separation zones obtained under various temperature distributions were then compared in term of Q_F, corresponding to unit productivity. All calculations in this study were performed on a DELL OPTIPLEX 380 personal computer equipped with a 2.6 GHz Intel Pentium dual-core processor.

Results and Discussion

SMBR productivity under various temperature distributions

In general, operating temperatures should be optimized together with flow rates using specified objective functions. For simplicity, we limited the temperatures to only four values, namely, 308, 313, 318 and 323 K. In addition, it was imposed that $T_j \geq T_{j-1}$, resulting in ascending adsorption strength from zone I to zone IV. It may be seen from Figure 2 that, when temperature is increased from 308 to 323 K, (1) Henry's constants decrease by moderate factors of 30%, 15 and 15%, for A, E and W, respectively, (2) the forward reaction rate significantly increases by a factor of 123%, and (3)

Table 2. Temperature Gradient Case of SMBR

					Optimal point		
Case	T_I (K)	T_{II} (K)	T_{III} (K)	T_{IV} (K)	m_{II}	m_{III}	Q_F^O (10^{-9} m^3/s)
1	308	308	308	308	0.644	0.870	2.32
2	323	323	323	323	0.537	0.964	4.98
3	323	323	318	318	0.544	0.900	4.17
4	323	323	313	313	0.553	0.844	3.40
5	323	323	308	308	0.562	0.800	2.78
6	318	318	308	308	0.585	0.822	2.65
7	313	313	308	308	0.612	0.846	2.50
8	318	318	313	313	0.576	0.870	3.30
9	323	318	313	308	0.577	0.843	3.10
10	323	323	323	308	0.535	0.962	4.98
11	323	318	318	308	0.567	0.900	3.88
12	323	313	313	308	0.605	0.840	2.75
13	323	308	308	308	0.650	0.797	1.72
14	323	318	308	308	0.586	0.800	2.50
15	323	313	308	308	0.616	0.799	2.13

the reaction equilibrium is barely changed due to the low ΔH_{rxn}.

In total, 35 among the 256 possible temperature distributions in the four operating zones satisfy the criterion of. Based on the consideration of both comprehensiveness and computational manageability, 15 representative cases (see Table 2) were investigated in this study by numerical simulations using the procedure described in the last section. Figure 3 shows that the obtained complete conversion and separation zones form typical triangle shape. The vertex of each triangle is the optimal operating point for the corresponding conditions since it has the maximum feed flow rate, which is proportional to the difference between m_{III} and m_{II} according to Eqs. 10 and 21. The obtained $Q_F{}^o$ values are also provided in Table 2, where the superscript o denotes optimal points. Table 2 shows that case 2, isothermally operated at the highest temperature, 323 K, has the highest $Q_F{}^o$ of 4.98×10^{-9} m^3 s^{-1}, whereas the other isothermal case (case 1) operated at 308 K gives a relatively low $Q_F{}^o$ of 2.32×10^{-9} m^3 s^{-1}. As a comparison, the typical gradient operation, case 9, uniquely featured by a distinguished temperature at each zone, gives a moderate $Q_F{}^o$ of 3.10×10^{-9} m^3 s^{-1}. Apparently, the adoption of temperature gradients does not necessarily improve the SMBR productivity. Furthermore, case 10, similar to case 2 except that T_{IV} is set to be the lowest temperature (308 K), also gives a $Q_F{}^o$ of 4.98×10^{-9} m^3 s^{-1} indicating that the SMBR productivity is insensitive to T_{IV}.

In order to evaluate the effects of temperature at different operating zones, $Q_F{}^o$ is separately plotted against them in Figure 4. Figure 4a and 4d show that that T_I and T_{IV} do not have direct effects on $Q_F{}^o$. The apparent trend that $Q_F{}^o$ increases with increased T_{III}, as shown in Figure 4c, indicates that T_{III} is a key operating parameter of this process. It is observed in Figure 4b that higher T_{II} is also favorable to enhance $Q_F{}^o$ but the effects are less significant than those of T_{III}. A deeper understanding of the thermal effects involves analysis of temporal and spatial distributions of different components along the SMBR unit at cyclic steady-state. Internal component concentration profiles at several time points within a switch are plotted in Figure 5 (case 2, optimal point). It is seen that reactant A is introduced to the SMBR system from the feed port and then moves along with the fluid to zone III, where the reaction is catalyzed. At the optimized flow rate (m_{III}), A is just about to breakthrough to the raffinate port by the end of a switch (1.0^- t_s), which meets the requirement of complete conversion and separation and fully uses the column length as well. After a switch operation, the previous zone III becomes the current zone II. In this zone, a fraction of reactant unconverted in zone III continues to react forming E and W. The less adsorbed E is conveyed by the fluid toward the feed port and enters zone III while the stronger adsorbate W is retained in the solid phase. After another switch operation, the above column becomes zone I. The previously adsorbed W is purged out by desorbent and collected at the extract port. In the meantime, adsorbent in the column is regenerated and ready to be used as zone IV in the next switch for the adsorption of uncollected E. The fact that all components are depleted from zone I and E does not breakthrough from section IV at 1.0^- t_s validate the choices of conservative multipliers in Eqs. 24 and 25. While simultaneous reaction and separation occur in both zones II and III, temperature effects in these two zones are rather different. As aforementioned, a higher-operating temperature corresponds to faster reaction rate and lower adsorption strength. Kinetically, a faster reaction rate is favorable in both zones. From the separation point of view, however, in order to achieve high productivity, weaker adsorption is preferred in zone II (lower m_{II}), while stronger adsorption is preferred in zone III (higher m_{III}). Therefore, temperature has synergy effects on kinetics and adsorption in zone II. Figure 5 shows that remained reactant A is completely converted in less than 0.7 t_s, whereas it takes the whole switch period for the fluid to drive product E out to the feed port, suggesting that zone II is dominated by separation process. In the case of zone III, on the other hand, temperature has contradicting effects on kinetics and adsorption. That reactant A is about to breakthrough to the raffinate port by the end of a switch indicates a kinetically controlled process, which is in agreement with our observations in a previous study.[24]

Effects of k_f

It has been shown in the previous section that the synthesis of methyl acetate is kinetically controlled and, as a result, nonisothermal operations do not display their potentials in the enhancement of SMBR productivity. In this section, we further examined the feasibility of applying nonisothermal conditions on similar systems with faster reaction rates. Simulations were carried out by keeping the other parameters constant while assuming that the forward reaction rate is multiplied by a factor of α (> 1).

We focused on four representative cases corresponding to monotonic temperature distribution (case 9), maximum temperature difference between sections II and III (case 5), and isothermal operations at lowest and highest temperatures (cases 1 and 2). For easy comparison among various operations, the productivity ratio is defined based on $Q_F{}^o$ obtained for case 2, which has the best performance in the previous section, i.e.

$$\beta_k = \frac{Q_F^O|_k}{Q_F^O|_2} \tag{26}$$

The calculation results are summarized in Table 3. It may be seen that when α is greater than 5, cases 5 and 9 under nonisothermal operations give higher productivities than case 2. In addition, case 5 with the highest

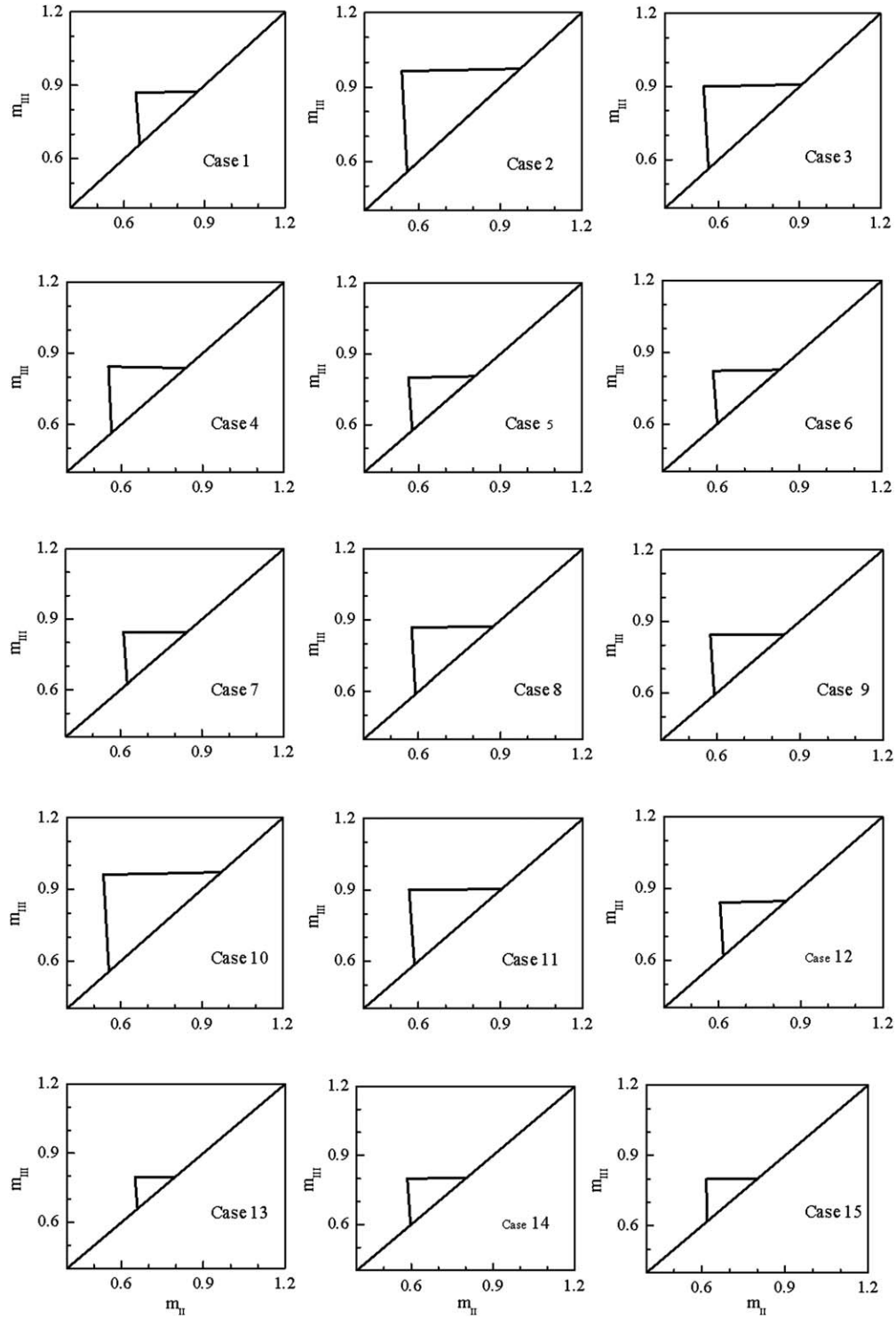

Figure 3. Calculated complete conversion and separation zones under various temperature gradients.

temperature difference between zones II and III has the highest β value. In the case of extremely fast reaction ($\alpha = 100$), the isothermal operation at lower temperature (308 K) also performs better than that at higher temperature (323 K), which is normally the case for isothermally operated SMB processes. All these observations indicate that the kinetic limitation is diminished with increased α and the overall SMBR process is dominated by product separation.

Figure 6 shows the effect of α on the obtained complete conversion and separation region for case 1. It is seen that the region is expanded with increased α. More specifically, the expansion is mainly along the m_{III} direction, while m_{II} is only slightly affected by α in the low-value range. This feature further validates the previous argument that zones II and III are dominated by separation and kinetics, respectively. When α is greater than 100, the region boundary approaches the one for pure separation, which was obtained by

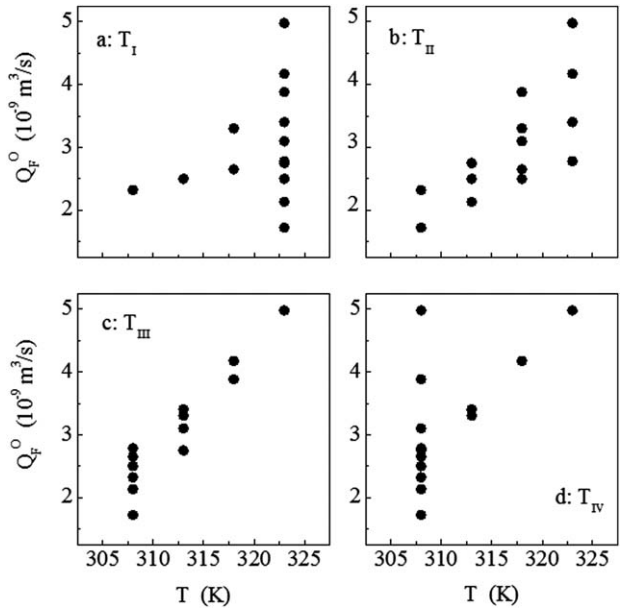

Figure 4. Q_F^O vs. operating temperature at different zones.

simulating an SMB process with an equimolar *E* and *W* solution (2.0×10^3 mol/m^3) as the feed. Noted is that the complete separation zone of SMB process is smaller than the one conventionally determined by the application of triangle theory[30] (dash line), which can be attributed to the finite theoretical stage number. This also points out the necessity of using a realistic model in the numerical simulation and optimization of SMB processes.

The internal concentration profiles of reactant *A* for three α values are plotted in Figure 7. When α is increased from 1 to 5, concentration of *A* drops faster in zone III, leaving a long tail toward the raffinate port. Also noticed is that, due to the higher m_{III}/m_{II} ratio, *A* in the feed is less diluted by the mixing with fluid from zone II, resulting in higher concentration

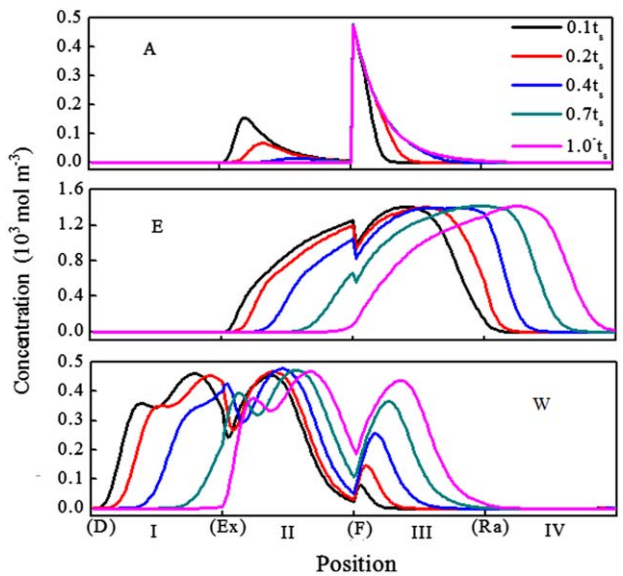

Figure 5. Internal concentration profiles at various times within a switch.

[Color figure can be viewed in the online issue, which is available at wileyonlinelibrary.com.]

Table 3. Effects of α Value on β (λ = 1)

	β				
Case	α=1	2	5	10	100
1	0.465	0.719	0.932	0.999	1.039
2	1.000 (0.23)[a]	1.000 (1.10)	1.000 (1.61)	1.000 (1.77)	1.000 (1.88)
5	0.559	0.777	1.059	1.161	1.227
9	0.622	0.835	1.029	1.092	1.133

[a]values in the brackets are Q_F^O of case 2, in the unit of 10^{-8} m^3/s

of *A* at the inlet. When α is further increased to 100, reaction rate becomes extremely fast and concentration of *A* drops dramatically to a level limited by local reaction equilibrium. This level off *A* front travels toward the raffinate port, forming a plateau by the end of a switch. Remained reactant in the column is further converted during the next switch (zone II) due to the separation of *E* and *W*. The concentration profiles of *E* and *W* are qualitatively similar to those in Figure 5, and are, therefore, omitted here for conciseness.

Effects of λ

As aforementioned in the model description section, λ is a model parameter characterizing the transient temperature change after a switch. Since it had been imposed that the temperature is descending from zone I to zone IV, according to the switch direction and Eq. 12, column temperature is increasing during the transient period after a switch operation. A larger λ value corresponds to a shorter transient period and should have qualitatively similar effects as that of a higher operating temperature.

An arbitrary value of 1.67×10^{-2} s^{-1} was used in all calculations involved in the above discussions. In order to examine the effects of λ, three cases, case 4 ($T_{II} > T_{III} = T_{IV}$), case 9 ($T_{II} > T_{III} > T_{IV}$), and case 10 ($T_{II} = T_{III} > T_{IV}$), were simulated for λ values of 0.5, 0.833, 1,67and 16.7 $\times 10^{-2}$ s^{-1}. Note that when *jpre* is I, *j* equals to IV. Since T_{IV} has no direct effects of on Q_F^O (see Figure 4d), T_I is not considered in this part of discussion. T_I is 323 K in all three cases. Using Eqs. 21 and 24 gives a t_s value of about 900 s, enough to complete the temperature transition for all λ values as shown in Figure 8. The coordinates of obtained vertices at

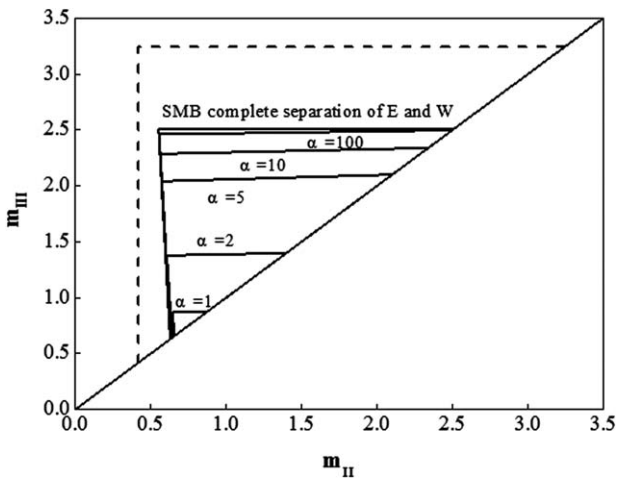

Figure 6. Effects of α on the complete conversion and separation zone (Case 1).

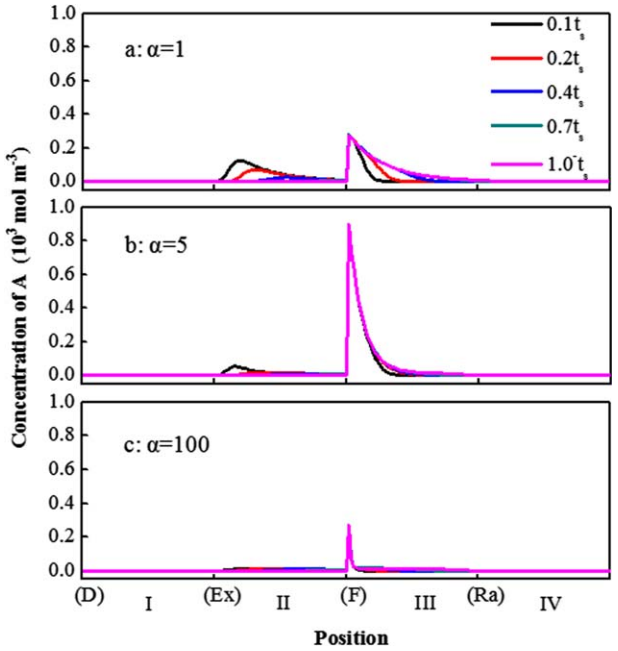

Figure 7. Internal concentration profile of component A for various α values.

[Color figure can be viewed in the online issue, which is available at wileyonlinelibrary.com.]

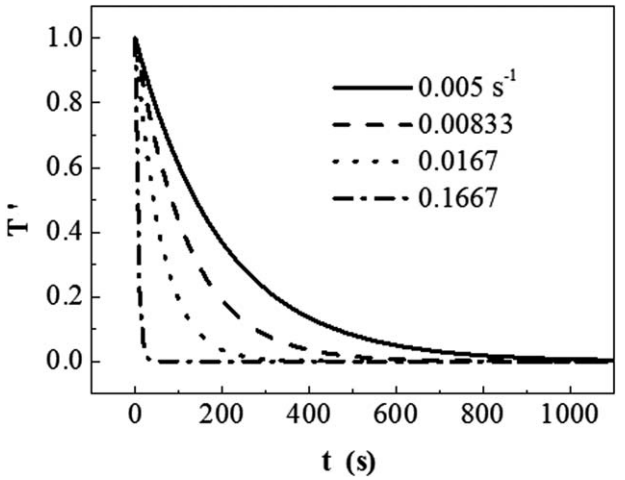

Figure 8. Transient temperature change after a switch for several λ values.

various λ values are summarized in Figure 9 for both $\alpha = 1$ (left column) $\alpha = 100$(right column).

First consider m_{II}, the flow rate in zone II where higher temperature is favorable for both kinetics and adsorption. For cases 4 and 9 with $T_{II} > T_{III}$, optimal m_{II} value decreases with increased λ for both slow ($\alpha = 1$) and fast ($\alpha = 100$)

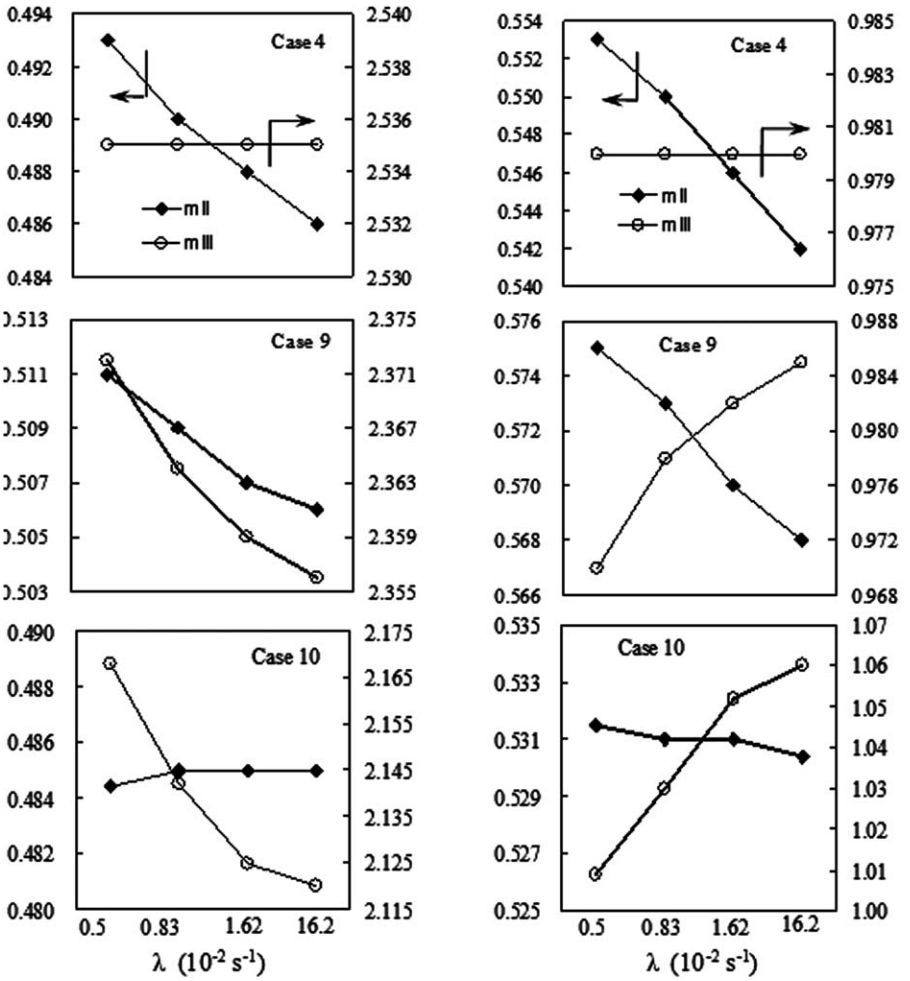

Figure 9. Effects of λ on m_{II} and m_{III} values of the obtained optimal points for cases 4, 9 and 10 (left column, α = 1, slow reaction; right column, α = 100, fast reaction).

Table 4. Calculation Results of 4 Representative Cases for Increased Henry's Constant of Component A

	T (K)							
case	*I*	*II*	*III*	*IV*	t_s (s)	m_{II}	m_{III}	Q_F^O (10^{-8} m^3/s)
1	308	308	308	308	1017	0.901	2.580	1.72
2	323	323	323	323	891	0.634	2.149	1.77
5	323	323	308	308	891	0.714	2.587	2.19
9	323	318	313	308	891	0.733	2.427	1.98

reaction rates due to the synergy temperature effects. For case 10 with $T_{II} = T_{III}$, a column does not experience a temperature rising after its switching from zone III to zone II. As a result, m_{II} is almost independent of λ.

The trends of m_{III} are different from those of m_{II} because temperature effects on kinetics and adsorption are contradicting in zone III. When T_{III} is higher than T_{IV} (cases 9 and 10), m_{III} increases with increased λ if the process is kinetically controlled ($\alpha = 1$). If reaction is fast ($\alpha = 100$), however, the kinetic limitation is diminished and the process becomes dominated by adsorption, resulting in decreased m_{III} with increased λ (cases 9 and 10). Similar to the trend of m_{II} for case 10, m_{III} is almost independent of λ for case 4 featured by $T_{III} = T_{IV}$.

Effects of Adsorption Strength of Reactant A. It may be noticed from Figure 2 that Henry's constant of reactant *A* is close to that of the light product *E*. In this section, simulations were carried out assuming that H^o_A is increased by a factor of 8, so that *A* has similar adsorption behaviors as *W*, the heavy product (see Figure 2a, the gray line). The equilibrium constant was decreased by the same factor accordingly to maintain the overall thermodynamic equilibrium. Other model parameters listed in Table 1 were kept constant. The same four representative cases as in the discussion of k_f effects were investigated and the results are summarized in Table 4. It may be seen that case 1, isothermally operated at the lowest temperature, has the lowest $Q_F{}^o$ and the optimal point is located at (0.90, 2.58) on the (m_{II}, m_{III}) plane. The optimal m_{III} value is almost identical to the one previously obtained for the SMB E/W separation process operated under the same temperature (see Figure 6), while m_{II} is significantly increased from about 0.6 to 0.9. Different from the trend of Figure 6 obtained using original parameters, in the case of increased Henry's constant of *A*, the triangle shape for SMBR mainly shrinks along m_{II} direction, indicating that zone II and zone III are controlled by kinetics and adsorption, respectively. The other isothermal operation at a higher temperature, 323 K, gives a slightly higher $Q_F{}^o$. $Q_F{}^o$ can be remarkably increased in the two nonisothermal cases and the best productivity is given by case 5 with the highest T_{II} and the lowest T_{III} allowed by the preset temperature range.

In previous sections, the evolution of spatial concentration profiles were used to elucidate temperature effects on SMBR productivity. A simpler explanation can also be given from the overall process point of view. When reactant *A* is less adsorbed, it is conveyed by the mobile phase toward zone III where the slow esterification mainly occurs. Increasing the reaction rate requires a higher temperature which, unfortunately, reduces the efficiency of heavy product *W* adsorption in zone III and, therefore, reduces the throughput of the SMB unit. On the other hand, if *A* is more strongly adsorbed and has a Henry's constant close to that of the heavy product *W*, *A* will be conveyed by the solid phase under proper operating conditions and has an overall movement toward zone II where, as shown in previous discussions, a higher temperature is favorable for both reaction and separation. In this case, the introduction of nonisothermal operation may exhibit its potential in the enhancement of SMBR productivity even for a system with slow reaction rate.

The discussion involved in this study is limited to the 4-column configuration. It is also acknowledged that, in addition to productivity, solvent consumption is another important variable for evaluating SMBR performance. In an ongoing systematic optimization study, solvent consumption will be considered as an objective function and effects of column distribution for multicolumn SMBR systems will be discussed.

Conclusions

In this work, we theoretically examined the feasibility of introducing nonisothermal operation into an SMBR system for the synthesis of methyl acetate. Using model parameters determined in a previous study, numerical simulations were carried out for an SMBR unit consisting of 4 columns and operated with various temperature distributions in the range of 308 K – 323 K. Optimal productivities of 15 representative cases were evaluated and compared under the constraints of complete conversion and complete product separation. The effects of kinetics and heat-transfer efficiency were also investigated. It was found that for this specific system, reactant *A* has Henry's constants close to those of the less adsorbed product *E* and the reaction mainly occurs in zone III. Temperature effects on adsorption and reaction are contradicting in zone III. When reaction rate is low, the system is kinetically controlled and T_{III} is the key parameter determining SMBR productivity. With increased reaction rate, kinetic limitation is diminished and the SMBR is operated more like an SMB for pure separation. In this case, nonisothermal operations display their potentials in improving SMBR productivity. Simulations also showed that when the reactant has Henry's constant close to that of the preferentially adsorbed product, it is carried by the solid phase and has an overall movement toward zone II. Since high temperature is favorable for reaction and separation in zone II nonisothermal operations can be applied to improve productivity. The findings presented in this work should be able to provide guidance for the future design and optimization of SMBR processes.

Acknowledgment

This work was supported by the National Natural Science Foundation of China (No.21106108) and Science Technology Department of Zhejiang Province (Qianjiang Grant, 2010R10043).

Notation

c = concentration in mobile phase, mol m^{-3}
d = column diameter, m
D_{app} = apparent dispersion coefficient in ED model, m^2 s^{-1}
E_f = activation energy, kJ mol^{-1}
H = Henry constant
k_f = forward rate constant, s^{-1}
K_{eq} = equilibrium constant, mol m^{-3}

L = column length, m
m = flow rate ratio defined in Eq. 21
M = mash point
N = number of theoretical plates
Pur = purity, %
q, q^* = dsorbed concentration in stationary phase, mol m^{-3}
Q = flow rate, m^3 s^{-1}
r = reaction rate, mol m^{-3} s^{-1}
R = universalgas constant, 8.314 J mol^{-1} K^{-1}
t = time, s
T = temperature, K
t_s = switching time, s
u_{int} = interstitial velocity in the packed column, m s^{-1}
V_{col} = column volume, m^3
z = axial coordination, m

Greek letters

α = multiplier of forward rate constant
β = productivity ratio defined in Eq. 26
ΔH_{ads} = adsorption enthalpy, kJ mol^{-1}
ΔH_{rxn} = reaction enthalpy, kJ mol^{-1}
ε = column voidage
φ = phase ratio
λ = characteristic value for transient temperature change, s^{-1}
υ = stoichiometric number

Subscripts and superscripts

0 = pre-exponential constants
I to IV = indices of columns
A = more adsorbed component; acetic acid
B = less adsorbed component
D = desorbent
E = methyl acetate
ex = extract
F = feed
i, j, k = indices of components, SMB operating zones and cases
O = optimized point
ra = raffinate
W = water

Literature Cited

1. Lode F, Houmard M, Migliorini C, Mazzotti M, Morbidelli M. Continuous reactive chromatography. *Chem Eng Sci*. 2001;56:269–291.
2. Dunnebier G, Fricke J, Klatt K. Optimal design and operation of simulated moving bed chromatographic reactors. *Ind Eng Chem Res*. 2000;39:2290–2304.
3. Ströhlein G, Assunção Y, Dube N, Bardow A, Mazzotti M, Morbidelli M. Esterification of acrylic acid with methanol by reactive chromatography: experiments and simulations. *Chem Eng Sci*. 2006;61:5296–5306.
4. Pereira CSM, Zabka M, Silva VMTM, Rodrigues AE. A novel process for the ethyl lactate synthesis in a simulated moving bed reactor (SMBR). *Chem Eng Sci*. 2009;64:3301–3310.
5. Zhang Z, Hidajat K, Ray AK. Application of simulated countercurrent moving-bed chromatographic reactor for MTBE synthesis. *Ind Eng Chem Res*. 2001;40:5305–5316.
6. Ray AK, Carr RW. Numerical simulation of a simulated countercurrent moving bed chromatographic reactor. *Chem Eng Sci*. 1995;50: 3033–3041.
7. Ray AK, Carr RW. Experimental study of a laboratory scale simulated countercurrent moving bed chromatographic reactor. *Chem Eng Sci*. 1995;50:2195–2202.
8. Ching CB, Lu ZP. Simulated moving-bed reactor: application in bioreaction and separation. *Ind Eng Chem Res*. 1997;36:152–159.
9. Zhang Y, Hidajat K, Ray AK. Modified reactive SMB for production of high concentrated fructose syrup by isomerization of glucose to fructose. *Biochem Eng J*. 2007;35:341–351.
10. Yu W, Hidajat K, Ray AK. Modeling, simulation, and experimental study of a simulated moving bed reactor for the synthesis of methyl acetate ester. *Ind Eng Chem Res*. 2003;42:6743–6754.
11. Azevedo DCS, Rodrigues AE. Design methodology and operation of a simulated moving bed reactor for the inversion of sucrose and glucose-fructose separation. *Chem Eng J*. 2001;82:95–107.
12. Minceva M, Gomes PS, Meshko V, Rodrigues AE. Simulated moving bed reactor for isomerization and separation of p-xylene. *Chem Eng J*. 2008;140:305–323. http://www.sciencedirect.com/science/article/pii/S1385894707006389 - cor1#cor1.http://www.sciencedirect.-com/science/article/pii/S1385894707006389 - cor1#cor1.
13. Lode F, M. Mazzotti, M. Morbidelli. Comparing true countercurrent and simulated moving-bed chromatographic reactors. *AIChE J*. 2003; 49:977–990.
14. Lode F, Francesconi G, Mazzotti M, Morbidelli M. Synthesis of methylacetate in a simulated moving-bed reactor: experiments and modeling. *AIChE J*. 2003;49:1516–1524.
15. Yu W, Hidajat KH, Ray AK. Application of multiobjective optimization in the design and operation of reactive SMB and its experimental verification. *Ind Eng Chem Res*. 2003;42:6823–6831.
16. Yu W, Hidajat KH, Ray AK. Optimization of reactive simulated moving bed and Varicol systems for hydrolysis of methyl acetate. *Chem Eng J*. 2005;112:57–72.
17. Pais LS, Rodrigues AE. Design of simulated moving bed and Varicol processes for preparative separations with a low number of columns. *J Chromatogr A*. 2003;1006:33–44.
18. Zhang Y, Hidajat K, Ray AK. Enantio-separation of racemic pindolol on α_1-acid glycoprotein chiral stationary phase by SMB and Varicol. *Chem Eng Sci*. 2007;62:1364–1375.
19. Hariprasad JS, Hidajat K, Ray AK. Optimization of reactive SMB and Varicol systems. *Comput Chem Eng*. 2003;27:1883–1901.
20. Migliorini C, Wendlinger M, Mazzotti M. Temperature gradient operation of a simulated moving bed unit. *Ind Eng Chem Res*. 2001; 40:2606–2617.
21. Jin W, Wankat PC. Thermal operation of four-zone simulated moving beds. *Ind Eng Chem Res*. 2007;46:7208–7220.
22. Abel S, Mzaaotti M, Morbidelli M. Solvent gradient operation of simulated moving beds I. Linear isotherms. *J Chromatogr A*. 2002; 944; 23–29.
23. Ziomek G, Kaspereit M, Jeżowski J, Seidel-Morgenstern A, Antos D. Effect of mobile phase composition on the SMB processer efficiency stochastic optimization of isocratic and gradient operation. *J Chromatogr A*. 2005;1070:111–124.
24. Yu W, Hidajat K, Ray AK. Determination of adsorption and kinetic parameters for methyl acetate esterification and hydrolysis reaction catalyzed by Amberlyst 15. *Appl Catal A: Gener*. 2004;260:191–205.
25. Guiochon G, Felinger A, Shirazi DG, Katti AM. Fundamentals of Preparative and Nonlinear Chromatography. 2nd ed. Boston, MS: Academic Press; 2006.
26. Traub HS. Preparative Chromatography. Germany: Weinheim: Wiley-VCH; 2005.
27. Horváth K, Fairchild JN, Kaczmarski K, Guiochon G. Martin-Synge algorithm for the solution of equilibrium-dispersive model of liquid chromatography. *J Chromatogr A*. 2010;1217:8127–8135.
28. Xu J, Zhu L, Xu G, Yu W, Ray, AK. Determination of competitive adsorption isotherm of enantiomers on preparative chromatographic columns using inverse method. *J Chromatogr A*. 2013;1273:49–56.
29. Abel S, Erdem G, Mazzotti M, Morbidelli M. Optimizing control of simulated moving beds-linear isotherm. *J Chromatogr A*. 2004;1033: 229–239.
30. Malek A, Farooq S. Hydrogen Purification from refinery fuel gas by pressure swing adsorption. *AIChE J*. 1998;44:1985–1992.
31. Xu J, Malek A, Farooq S. Production of argon from an oxygen-argon mixture by pressure swing adsorption. *Ind Eng Chem. Res*. 2006;45:5775–5787.
32. Rajendran A, Paredes G, Mazzotti M. Simulated moving bed chromatography for the separation of enantiomers. *J Chromatogr A*. 2009;1216:709–738.

Manuscript received Jan. 8, 2013, revision received May 27, 2013, and final revision received Aug. 9, 2013.